WILEY-VCH

DOI: 10.1002/ ((please add manuscript number))
Article type: Full Paper

Retorting Photocorrosion and Enhanced Charge Carrier Separation at CdSe Nanocapsules by Chemically Synthesized TiO_2 Shell for Photocatalytic Hydrogen Fuel Generation

Vempuluru Navakoteswara Rao, Sudhagar Pitchaimuthu, Parnapalle Ravi, Marappan Sathish, Hyungkyu Han, and Shankar Muthukonda Venkatakrishnan**

Mr. Vempuluru Navakoteswara Rao, Prof. Dr. Shankar Muthukonda Venkatakrishnan
Nanocatalysis and Solar Fuels Research Laboratory,
Department of Materials Science & Nanotechnology, Yogi Vemana University,
Kadapa-516005, Andhra Pradesh, India.
E-mail: shankar@yogivemanauniversity.ac.in

Dr. Sudhagar Pitchaimuthu,
Multifunctional Photocatalyst and Coatings Group, SPECIFIC, Materials Research Centre,
College of Engineering, Swansea University (Bay Campus), Fabian Way, Crymlyn Burrows,
Swansea SA1 8EN, Wales, United Kingdom.
E-mail: s.pitchaimuthu@swansea.ac.uk

Mr. Parnapalle Ravi, Dr. Marappan Sathish,
Functional Materials Division, Central Electrochemical Research Institute (CSIR-CECRI),
Karaikudi-630003, Tamil Nadu, India.

Dr. Hyungkyu Han
Los Alamos National Laboratory, Los Alamos, NM 87545, USA

Abstract:

Metal chalcogenide-based semiconductor nanostructures are promising candidate for photocatalytic or photoelectrocatalytic hydrogen generation. In order to protect CdSe from photocorrosion, a layer of TiO_2 wrapped (shell) onto CdSe (core) nanocapsule via the post-synthesis process. The morphology studies confirm that a thin crystalline TiO_2 shell (3-8 nm) wrapped in all the three directions onto CdSe core and thickness of the shell can be controlled through modulating titania precursor concentration. The feasibility of pristine CdSe nanocapsules and CdSe@TiO_2 in transforming visible light to hydrogen conversion was tested through photocatalysis reaction. The CdSe@TiO_2 nanocapsules generating a four-fold high rate of hydrogen gas (21 $mmol.h^{-1}.g^{-1}cat$) than pristine CdSe. In order to understand the role of shell@core, we have examined photoelectrochemical and impedance analysis. The CdSe@TiO_2 nanocapsules showed high photoelectric current generation and less charge

transfer resistance at electrode/electrolyte interfaces compared to pristine CdSe. These studies endorse that chemically synthesized crystalline TiO_2 shell played a multifunctional role in (a) surface passivation from photocorrosion, (b) promoting photocharge carrier separation via tunneling process between CdSe and TiO_2 interface. As a result, CdSe@TiO_2 nanocapsules showed a high conversion efficiency of 12.9% under visible light irradiation (328 $mW.cm^{-2}$) and turn over frequency is 0.05018 s^{-1}.

Introduction

Hydrogen (H_2) can be considered as sustainable, non-polluting, viable alternative fuel to replace fossil fuels and overcome the present and future energy crisis. Because, it is a carbon-free, light weight with higher energy density, eco- friendly and can be easily stored and transported compared to fossil fuels. [1–4] Power-free photocatalytic water splitting using semiconductor and natural Sunlight enable a secure energy system with reduced fossil fuel dependence. [5] For the last two decades, a wide variety of nanostructured semiconductor photocatalysts have been developed including metal, TiO_2/metal oxides and metal chalcogenides. [6–11] In the solar spectrum, major light photons (~55%) falls in visible spectrum. Therefore, narrow band gap energy (E_g = 1.5 to 2.0 eV) based metal chalcogenides received great attention in solar to hydrogen fuel conversion.

Among the narrow band gap semiconductors, cadmium based chalcogenides showed effective photocatalytic-to-hydrogen fuel generation compared to metal oxides as it possess high photo absorption in visible spectrum [12–24], In this line, cadmium selenide (CdSe) is a promising visible light driven semiconductor photocatalyst material have suitable energy gap and band edge potentials for H_2 generation via water splitting.[25,26] Cadmium selenide conduction band reduction potential lies between -0.27 eV to -1.26 eV and valence band oxidation potential is +0.7 eV to +1.42 eV, that fulfil the basic requirement of overall water splitting reactions. However, in view of improving the photocharge carrier separation at CdSe/electrolyte interfaces, co-

catalyst or secondary photo absorbers were randomly attached to CdSe surface. For instance, Pt deposited CdSe/CdS quantum dots nanocomposites, [27–29] CdSe-Au hybrid nano-dumbbells, [15,30] CdSe/MoS_2, [31] CdS/CdSe, [32–35] TiO_2/CdS/CdSe, [36,37] CdSe/ZnS[38] and CdSe-Ni_2S_3. [23] Besides improvedphotoabsorption in wide spectrum, poor charge separation properties of these materials, showed inadequate stability under prolonged light irradiation. The exposure of partially covered CdSe surface to electrolyte favors photocorrosion process, which affects stability of the CdSe and lowers overall H_2 fuel generation. The wrapping of CdSe with metal oxide in all three directions can protect the core from direct contact with reaction solution thus core@shell material overcomes photocorrosion issue. It is reported that TiO_2 shell layer coating onto CdSe quantum dots protect the photocorrosion issue at iodide based redox reactions. [31,39–41] Because TiO_2 is well known for high chemical stability in wide range of pH values. Also, its wide band gap nature (3.2 eV) allows as optical window to access the visible region in solar spectrum[42–44] to the primary photoabsorber besides it serves as co-catalyst. The wrapping of thinlayer (4 nm) TiO_2 layer (i) simultaneously protects the primary photocatalyst/photoabsorber for several hours as well as (ii) conducting the photocharge carriers to the electrolyte by tunnelling process. Recent demonstration on atomic layer deposited thin TiO_2 conformal layer effectively protects the Si photocathode and other photocatalyst from the photocorrosion process. [45] This encourages wrapping of thin TiO_2 onto the photocatalyst surface can increase the charge separation and overwhelming the photocorrosion issue at catalyst/electrolyte interfaces. Neverthless, the material processing cost by atomic layer deposition technique limits the large scale applications. Perhaps developing chemical method to wrap up a thin layer of TiO_2 over desired photocatalyst could reduce the materials cost, but controlling shell thickness is critical. Therefore, establishing low-cost material synthesis technique with thickness

controllability for thin conformal shell onto the core is high demand in chalcogenide based photocatalytic H_2 fuel generation.

One dimensional (1-D) nanostructures have a high internal surface area, amplifying optical pathways through multiple scattering, and unidirectional photocharge carriers flow point of charge injection to the electrolyte compared to the particulate structure. These advantages foster effective charge carriers generation, charge transport, and catalytic sites at 1-D nanostructures thus results in high photocatalytic H_2 production[46–48],

Recent review reports explore the advantages of 1-D nanostructures in materials properties and photocatalytic applications. [49] In this line, significant research has been progressed on 1-D metal oxide nanostructure-based solar-to-fuel generation, but 1-D metal chalcogenides based reports are scare.

It is anticipated that 1-D CdSe nanostructures wrapped with a thin TiO_2 shell layer prepared by the less expensive method will be promising for sustainable H_2 generation. To the best of our knowledge, for the first time, we demonstrate chemically synthesized thin TiO_2 shell wrapped with CdSe nanocapsules in photocatalytic visible light-to-H_2 fuel generation (**Scheme 1**). The benchmark photocatalyst consists of CdSe@TiO_2 nanocapsules were achieved by tuning TiO_2 shell thickness by varying the TTIB precursor concentration. The 1-D CdSe nanocapsules coated with TiO_2 showed a high rate of H_2 generation 40.6 $mmol.h^{-1}.g^{-1}_{cat}$ under UV-visible light and 23.2 $mmol.h^{-1}.g^{-1}_{cat}$ under visible light irradiation. Recyclability test of optimized CdSe@TiO_2 nanocapsules showed continuous H_2 generation upto 120 h for 4 cycles under visible light irradiation imply excellent photostability.

Results and Discussion

Figure 1 shows XRD pattern of pristine TiO_2, CdSe, and CdSe@TiO_2 (CST-1, CST-2, CST-3 CST-4, CST-5) core@shell photocatalysts. The diffraction peaks of CST-1 to CST-5 at 2θ values of 23.9, 25.4, 27.4, 29.7, 35.3, 42.2, 45.5, 49.7, 64.1 and 72.1° corresponds to (100), (002), (101), (102), (110), (103), (112), (203), (210) and (211) planes of wurtzite CdSe and anatase TiO_2 respectively. These results indicate that the products are single phases with lattice parameters of a= 4.29 Å, and c= 7.01 Å which is in line with standard values of CdSe (JCPDS Card No: 77-2307) and anatase TiO_2(JCPDS Card No: 21-1272). [12,50] Furthermore, in the case of CdSe@TiO_2 (CST-1 to CST-5) the peak intensity of crystalline CdSe is decreases with increasing TTIB concentration which indicates the TiO_2 crystal growth onto CdSe surface. The same result also implies that at thick-layer of TiO_2 shell wrapped onto CdSe does not allow light to scatter (*vide infra*) and hence overlapping of TiO_2 (101) crystal plane at 25.4° with (002) crystal plane of CdSe is observed. Further clarifying this point we have recorded Raman spectra. Figures (S1a – S1d) display the Raman spectra of the pristine CdSe, TiO_2 and CdSe/TiO_2 nanocomposites. In Figure S1c, mainly four major peaks are noticed at 195, 400, 595 and 620 cm^{-1} ascribed to Eg, A1g, B1g and Eg, which indicates that TiO_2 layer is in anatase crystal phase. Further from Figure S1a, it is observed that increasing TTIP precursor concentration influencing Raman peak shift (cm^{-1}) and peak intensity might due to increment of TiO_2 shell thickness. Here, it is worthy to refer the augment by Tian and co-workers on enhancement of intensity of E_g peak at CdSe/ TiO_2 samples indicates the crystalline nature of TiO_2. [51] Kim et al.,[52] ensured annealing treatment at above 230 °C can transform the anatase TiO_2 which coated on CdSe quantum dots. Similarly, the observed strong Eg peak indicates the crystalline nature of TiO_2 in CST-1 CST-5 catalysts. Figure 2a displays TEM image of pristine CdSe it infers nanocapsules morphology with an average diameter of 14 nm exists. Figures 2b - 2c shows HR-TEM images at 10 nm scale which clarifies the inter

planer distance is measured as 0.32 nm and 0.35 nm, which corresponds to the (101) and (002) planes of the wurtzite crystal structure of CdSe as shown in SAED pattern (Figure 2d) and it is in-line with XRD results.

The estimated d-spacing values of CdSe nanocapsules is well matched with literature reports.[53] Further, detailed structural information of the TiO_2 layer wrappted 1-D CdSe is examined by TEM images (Figures 2e - 2f). The thickness of the TiO_2 shell prepared by 0.4 mL TTIB (CST-1) (Figure S2a) and 0.8 mL (CST-2) (Figure 2e) is found to be 4 nm. However, the polycrystalline patterns of CdSe are still visible at CST-1 (Figure S2b), but it is false in the case of CST-2 (Figure S2c). This implies coverage of TiO_2 shell on CdSe surface has improved by increasing the TTIB volume from 0.4 mL to 0.8 mL.

Furthermore, the thickness of the TiO_2 shell layer is found to be increased from 4 nm to 12 nm by increasing TTIB volume from 0.8 mL to 2 mL (Figures 2f and S2) With increase in TTIP concentration, partial change in nanocapsule to spherical morphology is attributed due to significant change in chemical composition of solution mixture. This change may affect the pH of reaction solution thus included the nucleation and particle morphology. This observation strongly convinced that TTIB volume play a key role on thickness and coverage of TiO_2 shell layer onto CdSe surface. Figure S3a-S3f shows Energy-dispersive X-ray spectrum (EDAX) of all six fresh catalysts along with their elemental composition in percentage. This data explains that amount of cadmium present in core-shell material (CST-1 to 5) decreases monotonously from 30 to 7% with added titania precurosor. On the otherhand, increase in concentration of titania precursor raised the amount of Ti from 28 to 50% in CST-1 and CST-2 respectively. Further, increase in titania concentration has showed little influence on the amount of Ti that is 46,47 and 52 % for CST-3,4,5 respectively. Hence, it is

clarified that Ti-loading directly influenced that CST-1 and CST-2, whereas further increase in Ti-loading which influence the reacton parameters and limited the formation of TiO_2 in core-shell material. These data is in-line with TEM analysis as reported in Figure 2 and Figure S2.

Figure S4 displays FT-IR spectra for CdSe NC and CdSe@TiO_2 (CST-1, CST-2, CST-3, CST-4, CST-5) core@shell photocatalyst. From Figure S4, four major peaks are observed at 643, 1639, 1328, and 3418 cm^{-1} corresponds to Ti-O, C-H, Cd-Se and OH^- functional groups. [54,55] The spectral intensity of CdSe-TiO_2 nanocomposite is relying on the volume of TTIB concentration, where the high concentration of TTIB lowers CdSe peak which is in-line with SAED observation (Figure S2). This indirectly indicates the charge transfer possibility between -OH functional group of TiO_2 and Cd^{2+} ions of CdSe nanocapsule.[54–56] Further, chemical environment, and chemical state examined by using X-ray photoelectron spectroscopy (XPS).

Figure S5 depicts the full scan survey of the high-resolution spectra of the CdSe NC and CST-2 photocatalysts. Full survey scan spectra consists of C1s, Cd, Se, Ti, O elements and satellite peaks, which indicates PVP contains in nanocomposite material. [57] The core spectra of Cd3d, Se3d, Ti3d, and O1s are obtained from Figure S5b and presented in Figures 3a- 3d. From Figure 3a, Cd3d exhibits two major peaks at 405.4 and 412.1 eV which corresponds to Cd $3d_{5/2}$ and Cd $3d_{3/2}$ respectively. After TiO_2 shell coating, Cd $3d_{5/2}$ and Cd $3d_{3/2}$ peaks were shifted to lower binding energy direction indicates the lattice distortion by TiO_2. The Se3d core spectra (Figure 3b) of CdSe NC showed two distinguished peaks at 54.3 and 55 eV corresponds to $Se3d_{5/2}$ and $Se3d_{3/2}$, respectively. The Se3d spectrum shows broad and highly asymmetric under TiO_2 coating, which could be deconvoluted into two peaks corresponds to $Se3d_{5/2}$ and $Se3d_{3/2}$.

The similar broad features of Se3d spectrum were highlighted in recent reports. [17,58] The peak broadening may be due to several reasons including Se oxidation or Se^{2-} anionic species interaction with Ti-O lattice (Ti-O-Se). Ti 2p spectrum (Figure 3c) exhibits two distinguished peaks at 457.7 and 463.6 eV related to $Ti2p_{3/2}$ and $Ti2p_{1/2}$, respectively. The $Ti2p_{3/2}$ peak is further deconvoluted into two peaks 457.7 and 458.9 eV corresponds to Ti^{3+} and Ti^{4+}, respectively. The O1s spectrum is a footprint of oxygen vacancies, and hydroxyl groups exist from TiO_2 surface. From Figure 3d, The broad O1s spectrum deconvoluted into three peaks. The peak at 529.4 and 530.6 eV implies the oxygen species at Ti-O lattice. The additional small peak appeared at 532.2 eV attributed to hydroxyl group (O-H) presence on the TiO_2 surface. The observed chemical bonding between CdSe and TiO_2 is in good agreement with FTIR results and other previous reports. [58,59],

The surface structure of TiO_2 shell in CdSe@TiO_2 and CdSe NC are examined using nitrogen adsorption-desorption measurements. As shown in Figures S6a – S6b, CdSe@TiO_2 exhibits a type IV isotherm and high porosity compared to pristine CdSe. This is attributed to the mesoporous structure of TiO_2 wrapped on CdSe core. The pore-size distribution is estimated as 21±2 nm in diameter. The specific surface area of pristine CdSe NC and optimized CST-2 are presented in Figures S 6a-S6b. The specific area of CdSe NC and CST-2 are 2.5 and 10.5 m^2/g, respectively. The high surface area of CdSe@TiO_2 indicates more number of catalytic active sites triggers results in enhanced hydrogen fuel generation.

The diffused reflectance spectra of pristine CdSe and CdSe@TiO_2 nanocomposites (CST-1, CST-2, CST-3, CST-4, and CST-5) are presented in Figure 4. The CdSe NC shows broad absorption in the visible range between 400-690 nm.

The photocatalytic experiments were carried out using pristine CdSe NC and CST catalysts using 0.3 M of aqueous Na_2S and Na_2SO_4 sacrificial agent. Under the dark

condition, there is no H_2 gas detected from the reaction vessel. A significant amount of H_2 gas generation was observed only under light irradiation. This indicates the photocatalytic characteristic of CdSe and CdSe@TiO_2 hierarchical nanostructure associate with white light illumination. Theoretically, conduction band edge of CdSe lies above 0 V NHE which is favourable for reducing protons into H_2 gas generation.

Under light irradiation, the CdSe generate photoelectrons (e^-) and photohole (h^+) at conduction band, and valence band, respectively. Here, a mixture of Na_2S and Na_2SO_4 the solution acts as the hole scavenger. The possible routes for scavenging the holes are as follows, [8,12,60]

$$SO_4^{2-} + H_2O + 2h^+_{vB} \rightarrow SO_5^{2-} + 2H^+ \quad (1)$$

$$2S^{2-} + 2h^+_{vB} \rightarrow S_2^{2-} \quad (2)$$

$$SO_5^{2-} + S_2^{2-} + 2h^+_{vB} \rightarrow S_2O_5^{2-} + S^{2-} \quad (3)$$

$$2H^+ + 2e_{CB}^- \rightarrow H_2 \quad (4)$$

The photohole reacts with water containing sulphide and sulphate ions and produce H^+ ions and polysulphate ions as oxidised intermediates. Finally, the photoelectrons at conduction band react with protons and produce H_2 gas.

The quantity of hydrogen gas generated from photocatalytic reaction (equation 4) using CdSe NC and CST photocatalyst was quantified by gas chromatography and summarized in Figure 5a. The results were categorized at two different light irradiation condition (white light (UV + visible) and visible light). From Figure 5 (a), the quantity of H_2 gas generated at CdSe nanocapsules (18.6 $mmol.h^{-1}.g^{-1}_{cat}$) is markedly increased about one fold after TiO_2 shell coating (CST-2: 40.6 $mmol.h^{-1}.g^{-1}_{cat}$). The enhanced hydrogen gas generation by TiO_2 shell layer coating by multiple reasons a) protecting CdSe from photocorrosion, b) increases the photocharge carrier separation at CdSe/TiO_2/electorlyte interfaces. Furthermore, the possiblity of surface states presence in the metal chalcogenide nanostructures interfaces[12] attracts photoelectron and

photoholes which leads charge recombination. It is anticipated that the TiO_2 shell layer coating onto CdSe could manage the surface states and lowers the charge carriers recombination rate. Among the CST samples, the CST-2 showed better photocatalytic H_2 generation and the performance rate in the order CST-2> CST-3> CST-4> CST-5> CST-1> CdSe NC.

As can be seen in TEM images, TTIB concentration plays a crucial role in photocatalytic performance by controlling the TiO_2 shell thickness. At low TTIB concentration (CST-1), the surface coverage of the TiO_2 shell layer may be inadequate leading to photocorrosion. In the case of high TTIB concentration (CST-3 to CST-5) thickness of the shell is too thick and it can impede the photocharge carrier transport from CdSe nanocapsules to electrolyte. Briefly, thin TiO_2 shell layer can transfer the photoelectrons from the host layer to the electrolyte through the tunneling process. [6,12,61–63] A similar type of results for different material was reported by Domen *et al.*,[64] where they have explained the effect of shell thicknesses on the core surface and concluded that the shell thickness of 3-20 nm the range was beneficial to enhance the H_2 production. Even thicker TiO_2 layer can also transfer photoelectrons through electronically "leaky" behaviour attributed to Ti^{3+} related mid band states. [16,21,35,65] But, surface states or oxygen vacancies presence in the TiO_2/CdSe or TiO_2/electrolyte interfaces could trap the photoelectrons or holes which lead charge recombination process and thus lower catalytic activity. [7,8,66]

It implies that dense layer of TiO_2 could produce a higher quantity of surface states than that of thin TiO_2 layer. However, further investigation on surface states at CdSe/TiO_2 layer using time-resolved optic spectroscopy tool will shed more light on this issue. [58,59] It is observed from Figure S2c the high TTIB concentration deforms 1-D shape CdSe nanocapsules into spherical morphology. This morphology transformation might influence charge transport at CdSe and lower photocatalysis

performance. Therefore, optimized TiO_2 shell thickness at CST-2 allows the photocharge carriers to the electrolyte by the tunneling process without sacrificing the catalytic sites against photocorrosion. Unexpectedly, the H_2 generation rate was significantly reduced after filtering the UV light irradiation to the reaction chamber. The Raman results ensure that TiO_2 shell have crystalline nature, therefore the fraction of H_2 generation is contributed from TiO_2 under UV light irradiation. Further, photocatalytic activity of TiO_2 shell layer is stopped by UV filter. Another plausible reason may exist from Mie scattering process. For instance, non- absorbed UV light photons by 1-D CdSe nanocapsules can be scattered which increase optical pathway at the photocatalysis reaction chamber leads to enhancement in activity. [55,59,67] However, CST-2 sample still showed appreciable photocatalytic performance in H_2 generation (21.2 $mmol.h^{-1}.g^{-1}_{cat}$) even after filtering the UV light. The reproducibility of H_2 gas generation from benchmarking photocatalyst CST-2 was examined by repeating the photocatalysis experiments for 4 cycles under visible light irradiation. Each experimental cycle consists of 30 h and the quantity of output H_2 gas from respective cycles was summarized in Figure 5b. From Figure 5b, it is clearly demonstrated that CST-2 showed stable H_2 production at different cycles. This stability is attributed to TiO_2 shell layer coating on the CdSe surface that effectively suppress the photo-corrosion. Figure 5b reveals the recyclability of the optimized photocatalyst comparison with pristine CdSe NC, here were carried out four cycles each cycle upto 30 h continuous UV-visible light irradiation. CST-2 core/shell was shows high volume of hydrogen generation (760 $mmol.h^{-1}.g^{-1}$ for 30 h) when exhibiting to CdSe NC (540 $mmol.h^{-1}.g^{-1}$ for 30 h), which indicates TiO_2 shell material exhibits excellent charge separation from CdSe core being shows superior photocatalytic efficiency.

The visible light-to-hydrogen fuel conversion efficiency (VHC) values was obtained at high light intensity 328 $mW.cm^{-2}$ helps to qualitatively examine

photocatalytic characteristics of chalcogenides semiconductors in H_2 fuel generation for long term photo-irradiation. The visible light-to-hydrogen fuel conversion efficiency (VHC) of all the photocatalysts were estimated through the equation (5).

The visible light to H_2 energy conversion efficiency (%) = {(Output energy as H_2)/(The energy density of incident visible light x Irradiated area)} x 100 **(5)**

$$=\{(\Delta G\ (H_2O) \times \text{Rate of } H_2 \text{ production}\}/\{(3600\times\text{visible light energy} \times\text{irradiated area})\} \quad \textbf{(6)}$$

whereas, Gibbs free energy (ΔG) for H_2O = 237 $KJmol^{-1}$, time (h) = 1 h (3600 sec), visible light energy density measured by power meter = 328 $mW.cm^{-2}$, irradiation area = 33 cm^2.

The observed rate of H_2 generation from CdSe NC and CdSe@TiO_2 catalysts and their corresponding *VHC* values are displayed in Figure 6. The TiO_2 shell layer coated CdSe nanocomposite (CST-2) showed four times high conversion efficiency (VHC = 12.9%) than that of CdSe NC (VHC =3.0%). Further, the experimental data reveals that *VHC* efficiency apparently influenced by TTIB concentration. Until 0.8 mmol of TTIB concentration, the *VHC* values are gradually increased and above this optimized concentration it turns to decrease significantly. This ensure that TiO_2 shell layer growth rely on TTIB concentration, which controls the overall performance. Though *VHC* value is overrated compared to standard solar light irradiation (100 $mW.cm^{-2}$), [12,33,68,69] the purpose of this work focuses on exploring the advantages of TiO_2 shell layer against photocorrosion issue and were calculated turn over frequency (TOF) for optimized photocatalyst followed by standard formula and achieved 0.05018 s^{-1}. ~~atom~~ $^{-1}$ (refer supporting information and Figure S7).

The excitons life-time in pristine and core-shell materials were examined using photoluminescence spectra from 300 to 600 nm. Figure 7 displays the PL spectra of pristine CdSe that displayed two peaks at 340 and 510 nm as minor and major sharp peak respectively. Similarly CST-2 showed two peaks but the peak intensity at 510 nm is drastically lowered that is ~ 2.6 folds than pristine CdSe, revealed the extended charge carrier life-time of optimized core-shell photocatalyst. Figure S8 displays PL spectra of pristine CdSe and core-shell CdSe/TiO_2, the charge carrier life-time in the following order CST-2≅ CST-3 > CST-5 > CST-4 > CST-1 > CdSe. These results demonstrate that excitons life-time is retarded in core-shell photocatalyst than pristine CdSe, whereas CST-2 displayed prolonged life-time among all the catalyst. [8,70]

Further we investigate chemical state analysis for used photocatalyst CST-2, here Figures 8a-8d shows corresponding peaks well matching with fresh catalyst (shown in Figures 3a-3d) which indicates more stable chemical state and composition with two another peaks are noticed that peaks are related to Sodium (Na-1s) and Sulfur(S-2s) (see in Figures 8e-8f) these are well matching with standard peaks and confirms sacrificial reagent ions contains in CST-2 used photocatalyst.

In order to decipher the role of TiO_2 shell coated on CdSe the charge transfer characteristics photoelectrochemical studies were carried out. The CdSe NC and CST-2 powders were transformed into thin films onto conducting glass and it was tested as photoanode in an electrochemical cell. Note that both electrode thickness are not identical. A small potential applied in the circuit, current generation at dark and light irradiation condition was recorded and presented in Figure 9a and Figure S9a. The current generation only under light irradiation ensures the photocatalytic activity of CdSe and CST. From Figure 9a, CST electrode results a steady photocurrent profile than that of CdSe (Supporting information, Figure S9a). In CST sample, the steady photocurrent profile pattern implies that the TiO_2 shell layer protects the CdSe surface

from photocorrosion process. Though filtering light irradiation less than 450 nm wavelength still significant steady state photocurrent profile is exhibiting from CST-2 sample. This explains that TiO_2 shell layer is performing as photocorrosion protection layer for CdSe under visible light irradiation.

The electrochemical impedance analysis is a promising approach to explore the charge transfer characteristics at electrode/electrolyte interfaces under light irradiation condition. [71–73] The Nyquist plots measured at CST electrodes in the presence and absence of 450 nm cut off filter were presented in Figure 9b. As explained above in Figure 9a, after filtering the light irradiation less than 450 nm wavelength the photocharge carrier generation only existing from the CdSe layer. Therefore, the diameter of the semicircle observed from Figure 9b provides the charge transfer resistance (R_{ct}) at CdSe/electrolyte (with 450nm cut off filter), and $CdSe/TiO_2$/electrolyte (no filter) interfaces. The experimental data are fitted with equivalent circuit and R_{ct} values are obtained. The estimated R_{ct} values CST electrodes in the presence and absence of 450 nm cut off filter are found to be 23,916 and 13,884 Ω, respectively. The less charge transfer resistance at the CST electrode (without 450 nm filter) could be ascribed to the reduced charge recombination rate by managing the surface states at CdSe through TiO_2 shell layer coating as well photoconduction property of TiO_2. Also, band bending formation at $CdSe/TiO_2$ interfaces lead type-II band alignment facilitates the photo-charge carrier separation from semiconductor to the electrolyte (Scheme 2). The proposed reaction mechanism augment is in line with photocatalytic hydrogen generation results presented in Table 1. In order to understand the stability of the CdSe sample without TiO_2 coating Nyquist plots of pure CdSe was measured at different duration of light irradiation (5 min and 30 min). The results were presented in Figure S9b. The estimated *Rct* value of pure CdSe at 5 min and 30 min

light irradiation conditions are approximately 4760 Ω and 7760 Ω, respectively. The increment of charge transfer resistance at pure CdSe by increasing light irradiation duration clearly indicates the photocorrosion process occurred without TiO_2 shell layer. In the case of CST-2 sample we didn't see significant change in Rct value at different duration of light irradiation.

Conclusions

In summary, low-cost CdSe@TiO_2 nanocapsules were successfully synthesized by surfactant mediated approach. The thickness of TiO_2 shell has controlled through modulating TTIB precursor concentration. At low TTIB concentration (CST-2) thin TiO_2 shell wrapped on CdSe that facilitated high photocatalytic hydrogen generation. Conformal TiO_2 shell coverage and effective photocharge carrier separation through electron leak or tunneling process promote the overall visible light to hydrogen fuel conversion efficiency of CdSe nanocapsules. A chemical bonding possibility between CdSe and TiO_2 through Ti-O-Se formation at CdSe@TiO_2 interfaces were ensured by XPS. This lead effective electron transfers from primary photocatalyst layer to the electrolyte. Electrochemical impedance analysis reveals that charge transfer resistance at CdSe is significantly reduced by TiO_2 shell layer by bottlenecking the recombination routes at surface states, and favourable band alignment process at CdSe@TiO_2 interfaces. The photocatalysis recyclability test ensures TiO_2 shell supports long term operation without sacrificing H_2 gas generation. As a result, TiO_2 shell wrapped on CdSe NC performed a four-fold high quantity of hydrogen gas (21 $mmol.h^{-1}.g^{-1}_{cat}$) generation compared to pristine CdSe NC (5 $mmol.h^{-1}.g^{-1}_{cat}$) with 12.9% visible light to H_2 fuel conversion efficiency under 328 $mW.cm^{-2}$ light intensity of visible light irradiation. This quantity is remarkably higher value compared to previous reports on state-of-the-art CdSe nanostructured photocatalysis in associate with heterostructures (CdS, WS_2, $BiVO_3$), co catalyst (Au, Pt, and Ni $(OH)_2$) and passivation layers (ZnS, TiO_2). The

generic approach of synthesizing metal oxide thin shell over 1-D semiconductor nanostructures can be adopted to design new photocatalyst or electro catalyst towards sustainable energy conversion and storage systems. It is anticipated that decoration of less expensive hydrogen evolution co-catalyst will further enhance the catalytic activity of CdSe@TiO_2 to achieve high quantum yield in solar to H_2 fuel generation.

Experimental Section

All chemicals were purchased in analytic reagent grade, and used as received without purification. Cadmium nitrate dihydrate ($Cd(NO_3)_2.2H_2O$, Sigma Aldrich), selenium powder (Se, Sigma Aldrich), ammonia solution (NH_3, Merck), hydrazine ($N_2H_4.2H_2O$), Deionized water, titanium tetra-isobutaoxide (TTIB, Sigma Aldrich), 2-propanol (H_7C_3OH, Merck), ethanol (99.9%, C_2H_5OH), acetonitrile (CH_3CN, Merck), polyvinyl pyrrolidone (PVP) were used for material preparation. Deionized water, sodium sulphate (Na_2SO_4, Merck), and sodium sulfide (Na_2S, Fisher Scientific) were used for photocatalytic H_2 production experiments.

Synthesis of CdSe nanocapsules

The synthesis procedure was adapted from previous published reports[53] with slight modifications of the reactants, reagents, and surfactant molar ratio followed by hydrothermal method. Initially, 0.1 M of cadmium nitrate di-hydrate was dissolved in 10 mL of ammonium solution and allowed continuous stirring for 15 min, labelled as A. In another beaker, 0.2 M of selenium powder was suspended in 10 mL of hydrazine ($N_2H_4.2H_2O$) colour changes observed from colourless to pink and was labelled as B. Then the contents in B was added dropwise into solution A with continuous stirring and the colour change observed from colourless to pink and continued the stirring for

another 30 min. Later the reaction mixture transferred into autoclave made-up of non-corrosive stainless steel and kept in an electric hot air oven at 200℃ for 2 h, after that we collected the brown color precipitate and washed with de-ionized water and finally washed with absolute ethanol. The final precipitate was oven dried at 80 ˚C for 12h.

Synthesis of CdSe@TiO_2 core@shell nanocomposite

The core-shell CdSe@TiO_2 nanocomposites were prepared by the modified wet chemical method. Initially 100 mg of synthesized CdSe powder was dispersed in the 50 mL ethanol and stirring for 15 min at room temperature. Then 80 mg of PVP was added into above solution, subsequently, 0.8 mL of TTIB along with 10 mL of absolute ethanol is added dropwise into above solution with continuous stirring for 2 h at 30°C. Further washing with water and absolute ethanol the precipitate was collected and transferred into the autoclave. Subsequently 1:3 molar ratio of the solvent mixture (ethanol and acetonitrile) was added into 100 mL autoclave and than kept in an electric hot air oven at 160 ˚C for 20 h. Finally, the precipitate was washed by following the above procedure, and dried at 80 ˚C for a period of 12 h. The TiO_2 shell thickness was modulated by changing volume of TTIB as 0.4, 0.8, 1.2, 1.6 and 2.0 mL and the prepared CdSe@TiO_2 materials are marked as CST-1, CST-2, CST-3, CST-4 and CST-5 respectively. Note that all powder samples were calcined at 450 °C for 4 h under argon gas flow.

Sample preparation and characterization details

The synthesized pristine CdSe and CdSe@TiO_2 with core@shell morphology are examined and interpreted to elaborate properties of material. XRD patterns were recorded at 2θ = 10-80° using X-ray diffractometer (BRUKER D8 ADVANCE). The

purity of photocatalyst was analyzed by using Fourier-transformation infrared spectroscopy (FT-IR). The DRS UV-visible spectrum of powder samples was investigated by UV-vis-NIR Spectrophotometer (Varian Cary 5000). Energy dispersive X-ray spectra (EDX), morphology and shell thickness were measured by using HRTEM (FEI Tecnai F20 S-Twin) operating at 200 kV. The oxidation state and chemical environment of the CST fresh and used composite were analyzed by using XPS (ESCALAB 250 Xi-XPS system) with Al Kα radiation.

Photocatalytic hydrogen production

A Kjeldahl-flask shaped photoreactor (200 mL) made-up of quartz having the single port on the top and provision to seal with rubber septum for degassing and sampling. Typically, photocatalyst (5 mg) was charged into the reactor and dispersed in aqueous solution (50 mL) containing inorganic sacrificial agent (0.3 M N_2S and Na_2SO_4) under magnetic stirring (30 min) in dark condition. The reactor was degassed under vacuum followed by purging with nitrogen gas (high purity, IOLAR grade) for 30 min in each stage. The Xenon arc lamp (ORIAL instruments, New Port Co., Ltd, USA) with UV cut off filter $\lambda > 420$ nm (FSQ-ND01) used for UV-visible and visible light irradiation. The photoreactor was placed at a fixed distance (14.5 cm) from the light source to have reproducible results. To avoid thermal effects due to infra-red light, cold water circulated through circular quartz disk that fitted at the exit of lamp house is well known to filter infra-red light. In order to check the long-term stability of catalyst for prolonged usage, the recyclability tests were carried out for 120 h having four equal cycles with each cycle continued for 30 h under visible light irradiation and the H_2 generation rate was calculated by taking average of 5 h data. Under identical conditions both control and blank (without catalyst) experiments are conducted. The identification and quantification of H_2 was performed for each hour by using Gas

Chromatograph (Shimadzu GC-2014) fitted with molecular sieve/5Å column and TCD detector under a constant flow of N_2 as carrier gas.

Photoelectrochemical and impedance measurements

The resultant CdSe and CST-2 powder was converted into paste using binders (terpineol and ethyl cellulose – Sigma Aldrich) as per the previous report. [74] This CST-2 paste is coated onto pre-cleaned fluorinated tin oxide (FTO) glass substrate (NSG TEC Pilkington) by doctor blade technique and sintered at 450°C for 30 minutes. The resultant CST-2 electrode was used as photoanode in the three electrode electrochemical cell. The Ag/AgCl (1 M KOH) and Pt wire was used as reference and counter electrode. 0.3 M of Na_2S and Na_2SO_4 aqueous solution is used as electrolyte. The Autolab PGSTAT 302N electrochemical station, and solar simulator (HAL 320, Asahi Spectra Ltd, Japan) was used for photoelectrochemical measurements. The chronoamprometry measurements were carried out under dark and 1 sun (AM 1.5) light irradiation condition. For filtering UV light, a 450 nm cut-off filter (Asahi Spectra Ltd, Japan) was used between solar simulator and PEC cell. Electrochemical impedance spectroscopy measurements were carried out in a three electrode configuration, applying 10 mV AC signal and scanning in a frequency range between 1 KHz and 1 Hz, at open circuit potential (-0.9 V Ag/AgCl).

Supporting Information
Supporting Information is available from the Wiley Online Library or from the author.

Acknowledgements
Authors gratefully acknowledge financial support from the Ministry of New and Renewable Energy (MNRE), New Delhi, India (No.103/227/2014-NT). V.Navakoteswara Rao gratefully acknowledges Council of Scientific Industrial Research (CSIR-SRF), New Delhi, India for financial support through fellowship (ACK 124480/12K18) to carryout Ph.D. program. The

S.P thanks Ser Cymru-II program for supporting Rising Star Fellowship through Welsh Government and European Regional Development Fund (80761-SU-102 (West).

Manuscript received: ((will be filled in by the editorial staff))
Revised manuscript received: ((will be filled in by the editorial staff))
Accepted manuscript online: ((will be filled in by the editorial staff))
Version of record online: ((will be filled in by the editorial staff))

Conflict of Interest

The authors declare that there is no conflict of interest

Keywords: CdSe · hydrogen generation · nanocapsules · photocatalyst · solar

References

[1] J. Yang, A. Sudik, C. Wolverton, D.J. Siegel, *Chem. Soc. Rev.* **2010**, *39*, 656–675. doi:10.1039/b802882f.

[2] H. Furukawa, O.M. Yaghi, *J. Am. Chem. Soc.* **2009**, *131*, 8875–8883. doi:10.1021/ja9015765.

[3] S. Sharma, S.K. Ghoshal, *Renew. Sust. Energ. Rev.* **2015**, *43*, 1151–1158. doi:10.1016/J.RSER.2014.11.093.

[4] X. Li, J. Yu, J. Low, Y. Fang, J. Xiao, X. Chen, *J. Mater. Chem. A.* **2015**, *3*, 2485–2534. doi:10.1039/C4TA04461D.

[5] Y. Shi, B. Zhang, *Chem. Soc. Rev.* **2016**, *45*, 1529–1541. doi:10.1039/C5CS00434A.

[6] H.J. Yun, H. Lee, N.D. Kim, D.M. Lee, S. Yu, J. Yi, *ACS Nano*. **2011**, *5*, 4084–4090. doi:10.1021/nn2006738.

[7] B. Han, S. Liu, N. Zhang, Y.J. Xu, Z.R. Tang, *Appl. Catal. B.* **2017**, *202*, 298–304. doi:10.1016/j.apcatb.2016.09.023.

[8] V. Navakoteswara Rao, N. Lakshmana Reddy, M. Mamatha Kumari, P. Ravi, M. Sathish, K.M. Kuruvilla, V. Preethi, K.Raghava Reddy, N.P. Shetti, T.M. Aminabhavi, M. V. Shankar, *Appl. Catal. B.* **2019**, *254*, 174–185. doi:10.1016/j.apcatb.2019.04.090.

[9] W. Zhou, F. Sun, K. Pan, G. Tian, B. Jiang, Z. Ren, C. Tian, H. Fu, *Adv. Funct. Mater.* **2011**, *21*, 1922–1930. doi:10.1002/adfm.201002535.

[10] W. Zhou, W. Li, J.Q. Wang, Y. Qu, Y. Yang, Y. Xie, K. Zhang, L. Wang, H. Fu, D. Zhao, *J. Am. Chem. Soc.* **2014**, *136*, 9280–9283. doi:10.1021/ja504802q.

[11] W. Hu, W. Zhou, K. Zhang, X. Zhang, L. Wang, B. Jiang, G. Tian, D. Zhao, H. Fu, *J.*

Mater. Chem. A. **2016**, *4*, 7495–7502. doi:10.1039/c6ta01928e.

[12] V. Navakoteswara Rao, N.Lakshmana Reddy, M. Mamatha Kumari, P. Ravi, M. Sathish, B. Neppolian, M.V. Shankar, *Mater. Res. Bull.* **2018**, *103*, 122–132. doi:10.1016/j.materresbull.2018.03.030.

[13] N. Lakshmana Reddy, V. Navakoteswara Rao, M. Mamatha Kumari, P. Ravi, M. Sathish, M.V. Shankar, *Mater. Res. Bull.* **2018**, *101*, 223–231. doi:10.1016/J.MATERRESBULL.2018.01.043.

[14] W. Wang, C. Jin, L. Qi, *Small*. **2018**, *14*, 1–10. doi:10.1002/smll.201801352.

[15] H. Wang, Y. Gao, J. Liu, X. Li, M. Ji, E. Zhang, *Adv. Energy Mater.* **2019**, *9*, 1–9. doi:10.1002/aenm.201803889.

[16] Y.P. Xie, Z.B. Yu, G. Liu, X.L. Ma, H.-M. Cheng, *Energy Environ. Sci.* **2014**, *7*, 1895–1901. doi:10.1039/c3ee43750g.

[17] L.Z.W. Li, Z.J. Li, J.J. Wang, X.B. Li, X.B. Fan, Q.Y. Meng, K. Feng, B. Chen, C.H. Tung, *Adv. Mater.* **2013**, *25*, 6613–6618. doi:10.1002/adma.201302908.

[18] J. Xu, L. Wang, X. Cao, *Chem. Eng. J.* **2016**, *283*, 816–825. doi:10.1016/j.cej.2015.08.018.

[19] Y. Lei, C. Yang, J. Hou, F. Wang, S. Min, X. Ma, Z. Jin, J. Xu, G. Lu, K.-W. Huang, *Appl. Catal. B.* **2017**, *216*, 59–69. doi:https://doi.org/10.1016/j.apcatb.2017.05.063.

[20] R. Bera, S. Kundu, A. Patra, *ACS Appl. Mater. Interfaces.* **2015**, *7*, 13251–13259. doi:10.1021/acsami.5b03800.

[21] J. Zhang, Y. Wang, J. Jin, J. Zhang, Z. Lin, F. Huang, J. Yu, *ACS Appl. Mater. Interfaces.* **2013**, *5*, 10317–10324. doi:10.1021/am403327g.

[22] X. Wang, X. Wang, J. Zhao, J. Song, C. Su, Z. Wang, *Chem. Eng. J.* **2018**, *341*, 516–525. doi:10.1016/j.cej.2018.02.054.

[23] H. Guan, S. Zhang, X. Cai, Q. Gao, X. Yu, X. Zhou, F. Peng, Y. Fang, S. Yang, *J. Mater. Chem. A.* **2019**, *7*, 2560–2574. doi:10.1039/c8ta08837c.

[24] W. Wang, S. Zhu, Y. Cao, Y. Tao, X. Li, D. Pan, D.L. Phillips, D. Zhang, M. Chen, G. Li, H. Li, *Adv. Funct. Mater.* **2019**, *29*, 1901958. doi:10.1002/adfm.201901958.

[25] J. Zheng, Y. Liu, G. Ji, P. Zhang, X. Cao, B. Wang, C. Zhang, X. Zhou, Y. Zhu, D. Shi, *ACS Appl. Mater. Interfaces.* **2015**, *7*, 23431–23438. doi:10.1021/acsami.5b07000.

[26] Y. Peng, L. Shang, T. Bian, Y. Zhao, C. Zhou, H. Yu, L.Z. Wu, C.H. Tung, T. Zhang, *Chem. Commun.* **2015**, *51*, 4677–4680. doi:10.1039/C5CC00136F.

[27] Z. J. Li, X.B. Fan, X.B. Li, J.X. Li, F. Zhan, Y. Tao, X. Zhang, Q.Y. Kong, N.J. Zhao, J.P. Zhang, C. Ye, Y.J. Gao, X.Z. Wang, Q.Y. Meng, K. Feng, B. Chen, C.H. Tung,

L.Z. Wu, *J. Mater. Chem. A.* **2017**, *5*, 10365–10373. doi:10.1039/C7TA01670K.

[28] F. Qiu, Z. Han, J. Peterson, M.Y. Odoi, K.L. Sowers, T.D. Krauss, *Nano Lett.* **2016**, *16*, 95347–5352. doi:10.1021/acs.nanolett.6b01087.

[29] A. Thibert, F.A. Frame, E. Busby, M.A. Holmes, F.E. Osterloh, D.S. Larsen, *J. Phys. Chem. Lett.* **2011**, *22*, 2688–2694. doi:https://doi.org/10.1021/jz2013193.

[30] R. Costi, A.E. Saunders, E. Elmalem, A. Salant, U. Banin, *Nano Lett.* **2008**, *8*, 637–641. https://doi.org/10.1021/nl0730514

[31] F.A. Frame, F.E. Osterloh, *J. Phys. Chem.C.* **2010**, *114*, 10628–10633. https://doi.org/10.1021/jp101308e

[32] Z.J. Li, J.J. Wang, X.B. Li, X. B. Fan, Q.Y. Meng, K. Feng, B. Chen, C.H. Tung, L.Z. Wu, *Adv. Mater.* **2013**, *25*, 6613–6618. doi:10.1002/adma.201302908.

[33] P. Wang, J. Zhang, H. He, X. Xu, Y. Jin, *Nanoscale*. **2015**, *7*, 5767–5775. doi:10.1039/C4NR07343F.

[34] A.G. Dukovic, M.G. Merkle, J.H. Nelson, S.M. Hughes, A.P. Alivisatos, *Adv.Mater*. **2008**, *20*, 4306–4311. doi:10.1002/adma.200800384.

[35] P. Wang, J. Zhang, H. He, X. Xu, Y. Jin, *Nanoscale*. **2014**, *6*, 13470–13475. doi:10.1039/C4NR04600E.

[36] Y. Lee, C. Chi, S. Liau, *Chem. Mater.* **2010**, *7*, 922–927. doi:10.1021/cm901762h.

[37] K. Li, M. Han, R. Chen, S. Li, S. Xie, C. Mao, X. Bu, *Adv. Mater*. **2016**, *28*, 8906–8911. doi:10.1002/adma.201601047.

[38] J. Huang, K.L. Mulfort, P. Du, L.X. Chen, *J. Am. Chem. Soc.* **2012**, *40*, 16472–16475. doi.:10.1021/ja3062584

[39] M.A. Holmes, T.K. Townsend, F.E. Osterloh, *Chem. Commun.* **2012**, *48*, 371–373. doi:10.1039/c1cc16082f.

[40] H.B. Kim, D.J. Jang, *Nanoscale*. **2016**, *8*, 403–410. doi:10.1039/c5nr06125c.

[41] L. Li, H. Lu, K. Deng, *J. Mater. Chem. A.* **2013**, *1*, 2089–2093. doi:10.1039/c2ta00410k.

[42] C. Chen, C. Chao, Z.H. Lang, *Chem. Mater.* **2000**, *12*, 1516–1518. doi:10.1021/cm9907920

[43] R.B. Kale, C.D. Lokhande, *Appl. Sur. Sci.* **2004**, *223*, 343–351. doi:10.1016/j.apsusc.2003.09.022.

[44] H. Shim, V.R. Shinde, J.W. Kim, T.P. Gujar, O. Joo, H.J. Kim, W.B. Kim, *Chem. Mater.* **2009**, *21*, 1875–1883. doi:10.1021/cm8034483

[45] Y. Li, G. Chen, Q. Wang, X. Wang, A. Zhou, Z. Shen, *Adv. Funct. Mater.* **2010**, *20*,

3390–3398. doi:10.1002/adfm.201000604.

[46] M. Ge, C. Cao, J. Huang, S. Li, Z. Chen, K.Q. Zhang, S.S. Al-Deyab, Y. Lai, *J. Mater. Chem. A.* **2016**, *4*, 6772–6801. doi:10.1039/C5TA09323F.

[47] D.Praveen Kumar, V. Durga Kumari, M. Karthik, M. Sathish, M.V. Shankar, *Sol. Energy Mater Sol. Cells.* **2017**, *163*, 113–119. doi:10.1016/j.solmat.2017.01.007.

[48] B.Y. Xia, P. Yang, Y. Sun, Y. Wu, B. Mayers, B. Gates, Y. Yin, F. Kim, H. Yan, Adv. Mater. **2003**, *15*, 353–389. doi:10.1002/adma.200390087.

[49] V.J. Babu, S. Vempati, *Phys. Chem. Chem. Phys.* **2015**, *17*, 2960–2986. doi:10.1039/C4CP04245J.

[50] L. Gu, J. Wang, H. Cheng, Y. Du, X. Han, *Chem. Commun.* **2012**, *48*, 6978–6980. doi:10.1039/c2cc33163b.

[51] F. Tian, Y. Zhang, J. Zhang, C. Pan, *J. Phys. Chem. C.* **2012**, *116*, 7515–7519. doi:10.1021/jp301256h.

[52] J.Y. Kim, S.B. Choi, J.H. Noh, S. Hunyoon, S. Lee, T.H. Noh, A.J. Frank, K.S. Hong, *Langmuir*. **2009**, *25*, 5348–5351. doi:10.1021/la804310z.

[53] Q. Peng, Y. Dong, Z. Deng, Y. Li, *Inorg. Chem.* **2002**, *41*, 5249–5254. doi:10.1021/ic0257266

[54] Y.C. Pu, H. Ma, N. Sajben, G. Xia, J. Zhang, Y. Li, J.Z. Zhang, *ACS Appl. Energy Mater.* **2018**, *1*, 2907–2917. doi:10.1021/acsaem.8b00563.

[55] A. Nikhil, D.A. Thomas, S. Amulya, S. Mohan Raj, D. Kumaresan, *Sol. Energy*. **2014**, *106*, 109–117. doi:10.1016/j.solener.2014.01.034.

[56] J.K. Cooper, A.M. Franco, S. Gul, C. Corrado, J.Z. Zhang, *Langmuir*. **2011**, *27*, 8486–8493. doi:10.1021/la201273x.

[57] S. Lee, K. Lee, W.D. Kim, S. Lee, D.J. Shin, D.C. Lee, *J. Phy. Chem. C.* **2014**, *118*, 23627–23634. doi:10.1021/jp508315m.

[58] P. Wang, X. Li, J. Fang, D. Li, J. Chen, X. Zhang, Y. Shao, *Appl. Catal. B.* **2016**, *181*, 838–847. doi:10.1016/j.apcatb.2015.08.046.

[59] P. Wang, D. Li, J. Chen, X. Zhang, J. Xian, X. Yang, X. Zheng, X. Li, Y. Shao, *Appl. Catal. B.* **2014**, *160–161*, 217–226. doi:10.1016/j.apcatb.2014.05.032.

[60] J. Schneider, D.W. Bahnemann, *J. Phys. Chem. Lett.* **2013**, *4*, 3479–3483. doi:10.1021/jz4018199.

[61] X. Chang, T. Wang, J. Gong, *Semicond. Semimet.* **2017**, *97*, 429–467. doi:10.1016/bs.semsem.2017.04.004.

[62] X. Yang, J. Xu, T. Wong, Q. Yang, C.-S. Lee, Phys. Chem. Chem. Phys. **2013**, *15*,

12688. doi:10.1039/c3cp51722e.

[63] N. Sakamoto, H. Ohtsuka, T. Ikeda, K. Maeda, D. Lu, M. Kanehara, K. Teramura, T. Teranishi, K. Domen, *Nanoscale*. **2009**, *1*, 106–109. doi:10.1039/b9nr00186g.

[64] K. Maeda, K. Teramura, D. Lu, N. Saito, Y. Inoue, K. Domen, *Angew. Chem. Int. Ed.* **2006**, *45*, 7806–7809. doi:10.1002/anie.200602473.

[65] Y. Liu, P. Zhang, B. Tian, J. Zhang, *ACS Appl. Mater. Interfaces*. **2015**, 7, 13849–13858. doi:10.1021/acsami.5b04128.

[66] N.Lakshmana Reddy, V.Navakoteswara Rao, M.Mamatha Kumari, M. Sathish, M.V. Shankar, *Int. J. Hydrog. Energy*. **2018**, *43*, 22315–22328. doi:10.1016/j.ijhydene.2018.10.054.

[67] W. Ho, J.C. Yu, *J. Mol. Catal. A*. **2006**, *247*, 268–274. doi:10.1016/j.molcata.2005.11.057.

[68] N. Buehler, K. Meier, J.F. Reber, *J. Phys. Chem.* **1984**, *88*, 3261–3268. doi:10.1021/j150659a025.

[69] N. Qin, J. Xiong, R. Liang, Y. Liu, S. Zhang, Y. Li, Z. Li, L. Wu, *Appl. Catal. B.* **2017**, *202*, 374–380. doi:10.1016/j.apcatb.2016.09.040.

[70] K.M. Lee, S.H. Chang, M.C. Wu, C.G. Wu, *Vib. Spectrosc.* **2015**, *80*, 66–69. doi:10.1016/j.vibspec.2015.08.001.

[71] B. Chong, W. Zhu, X. Hou, *J. Mater. Chem. A.* **2017**, *5*, 6233–6244. doi:10.1039/c6ta10202f.

[72] P. Brown, P. V. Kamat, *J. Am. Chem. Soc.* **2008**, *130*, 8890–8891. doi:10.1021/ja802810c.

[73] J. Yan, Q. Ye, F. Zhou, *RSC Adv*. **2012**, *2*, 3978–3985. doi:10.1039/c2ra01102f.

[74] P. Zhang, M. Fujitsuka, T. Majima, *J. Ener. Chem.* **2016**, *25*, 917–926. doi:10.1016/j.jechem.2016.11.012.

[75] Y. Chen, C.H. Chuang, Z. Qin, S. Shen, C. Burda, *Nanotechnology*. **2017**, *28*, 084002. doi:10.1088/1361-6528/aa5642

[76] F.A. Frame, E.C. Carroll, D.S. Larsen, M. Sarahan, N.D. Browning, F.E. Osterloh, *Chem. Commun.* **2008**, 2206–2208. doi:10.1039/b718796c.

[77] I. Grigioni, M. Bernareggi, G. Sinibaldi, M.V. Dozzi, E. Selli, *Appl. Catal A.* **2016**, *518*, 176–180. doi:10.1016/j.apcata.2015.09.021.

[78] R. Shi, Y. Cao, Y. Bao, Y. Zhao, G.I.N. Waterhouse, Z. Fang, L.Z. Wu, C.H. Tung, Y. Yin, T. Zhang, *Adv. Mater*. **2017**, *29*, 1–7. doi:10.1002/adma.201700803.

[79] Y. Zhong, Y. Shao, F. Ma, Y. Wu, B. Huang, X. Hao, *Nano Energy*. **2017**, *31*, 84–89.

doi:10.1016/j.nanoen.2016.11.011.

[80] D. Zhong, W. Liu, P. Tan, A. Zhu, Y. Liu, X. Xiong, J. Pan, *Appl. Catal. B.* **2018**, *227*, 1–12. doi:10.1016/j.apcatb.2018.01.009.

[81] P. Tongying, V.V. Plashnitsa, N. Petchsang, F. Vietmeyer, G.J. Ferraudi, G. Krylova, M. Kuno, *J. Phys. Chem. Lett*. **2012**, *3*, 3234–3240. doi:10.1021/jz301628b.

[82] Z. Wang, J. Wang, L. Li, J. Zheng, S. Jia, J. Chen, B. Liu, Z. Zhu, *J. Mater. Chem. A.* **2017**, *5*, 20131–20135. doi:10.1039/c7ta06085h.

[83] Y. Liu, F. Dai, R. Zhao, X. Huai, J. Han, L. Wang, *J. Mater. Sci.* **2019**, *54*, 8571–8580. doi:10.1007/s10853-019-03484-x.

[84] Y. Ji, W. Guo, H. Chen, L. Zhang, S. Chen, M. Hua, Y. Long, Z. Chen, *J. Phys.Chem. C.* **2015**, *119*, 27053–27059. doi:10.1021/acs.jpcc.5b09055.

[85] H. Wang, W. Zhu, B. Chong, K. Qin, *Int. J. Hydrog Energy*. **2014**, *39*, 90–99. doi:10.1016/j.ijhydene.2013.10.048.

[86] S. Yu, Z.J. Li, X.B. Fan, J.X. Li, F. Zhan, X.B. Li, Y. Tao, C.H. Tung, L.Z. Wu, *ChemSusChem*. **2015**, *8*, 642–649. doi:10.1002/cssc.201402885.

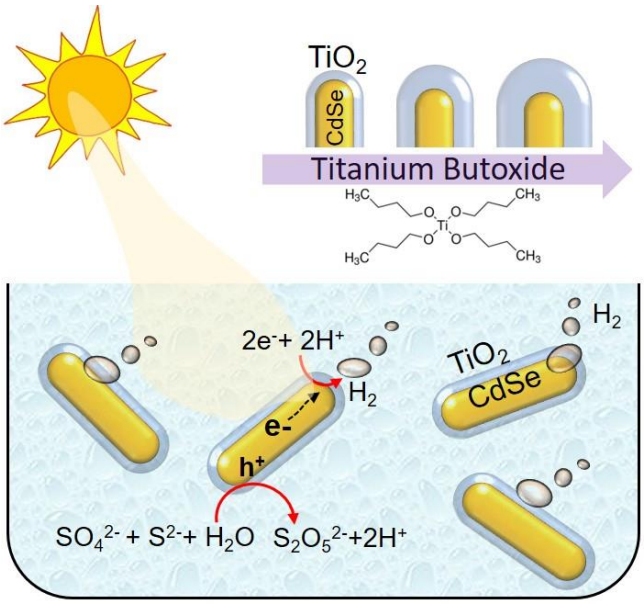

Scheme 1. Schematic illustration of photocatalytic hydrogen generation using TiO_2 @ CdSe nanocapsules under simulated solar light irradiation. TiO_2 shell thickness can be tailored by modulating titania precursor (TTIB) concentation.

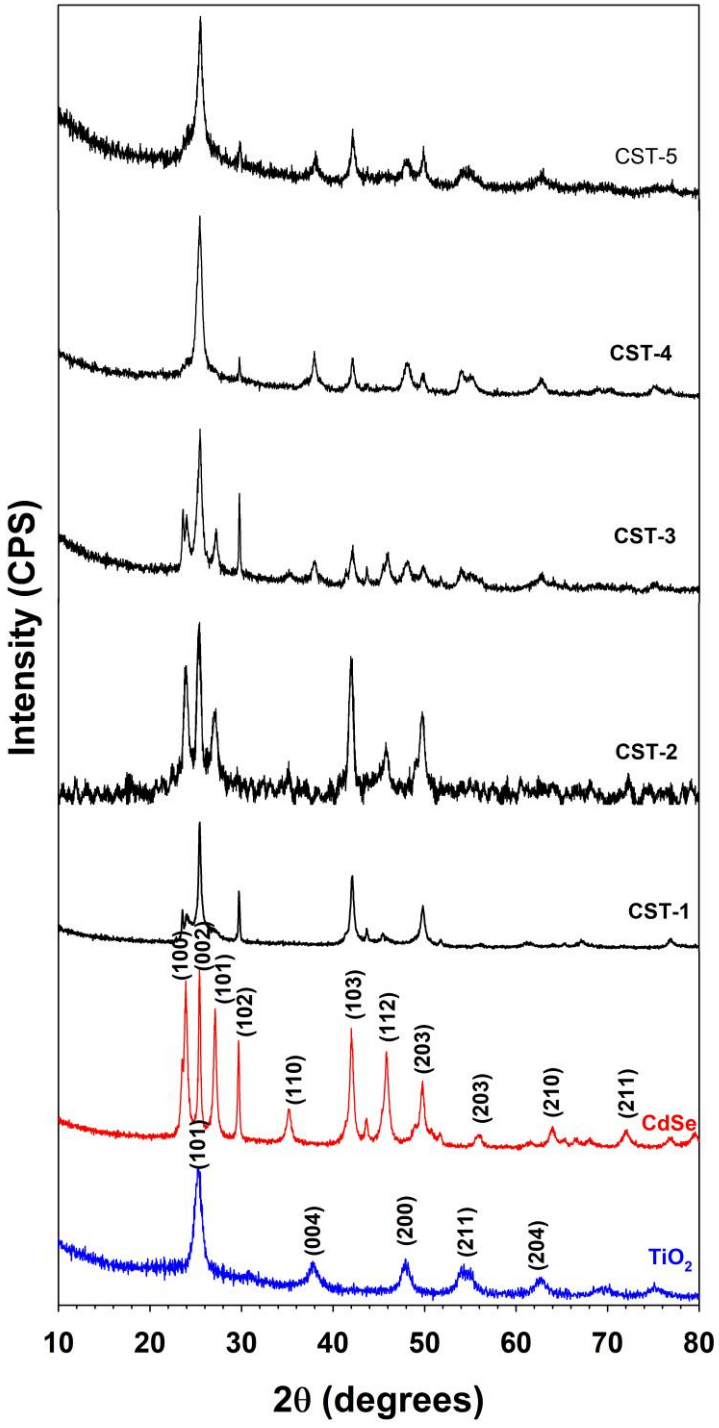

Figure 1. XRD pattern of TiO_2, CdSe and CdSe@TiO_2 photocatalysts (CST-1, CST-2, CST-3, CST-4 and CST-5).

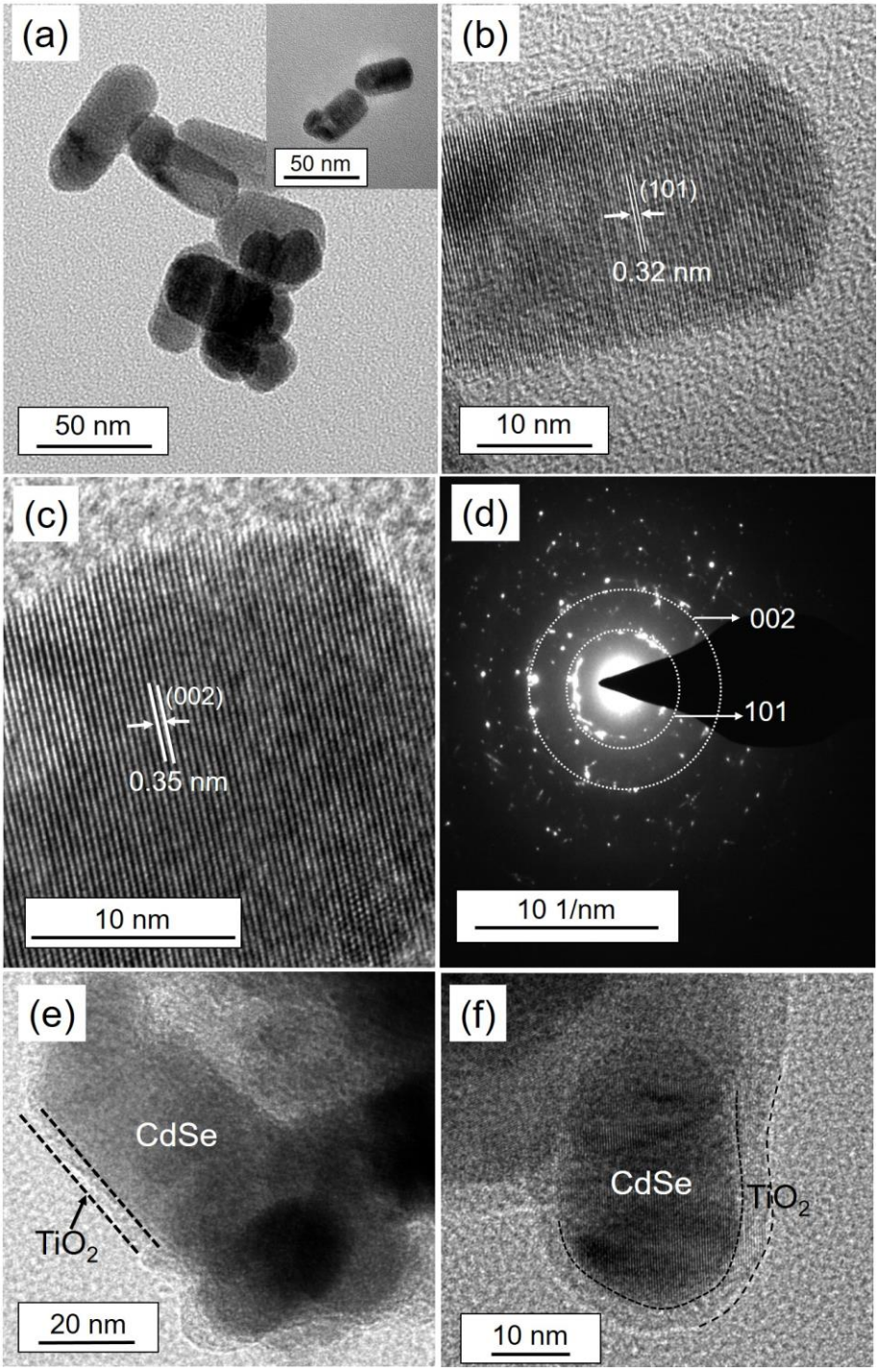

Figure 2. High resolution TEM images of CdSe; a) at 50 nm scale; b-c) at 10 nm scale; d) Selected area electron diffraction (SAED) pattern of CdSe nanocapsules; e-f) High resolution TEM images of CdSe@TiO_2 (CST-2 and CST-5) nanocomposite at 20 nm scale recorded in same sample at different locations.

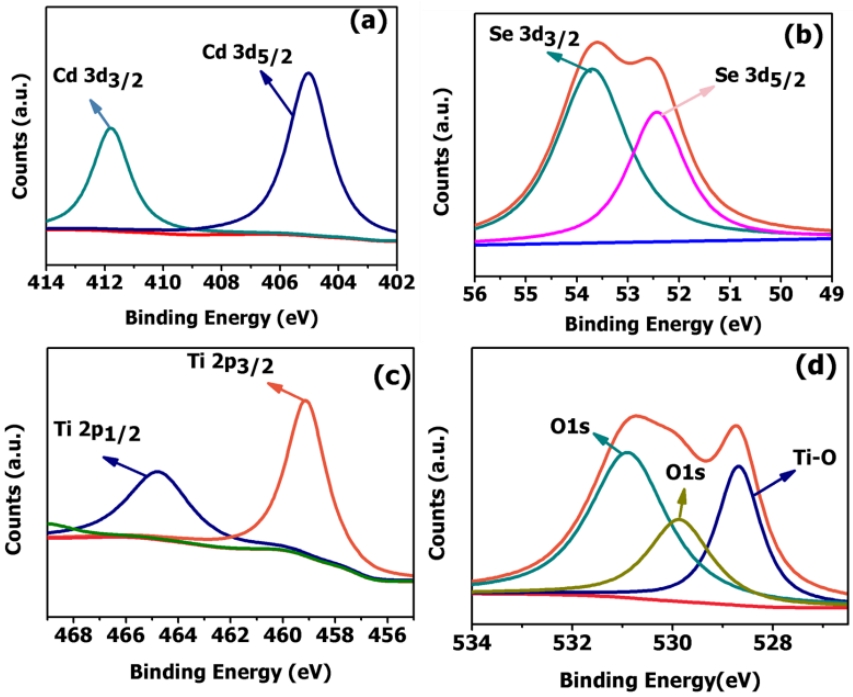

Figure 3. XPS profile of TiO_2 shell coated CdSe (CST-2); a) Cd3d; b) Se 3d; c) Ti2p and d) O1s core spectra.

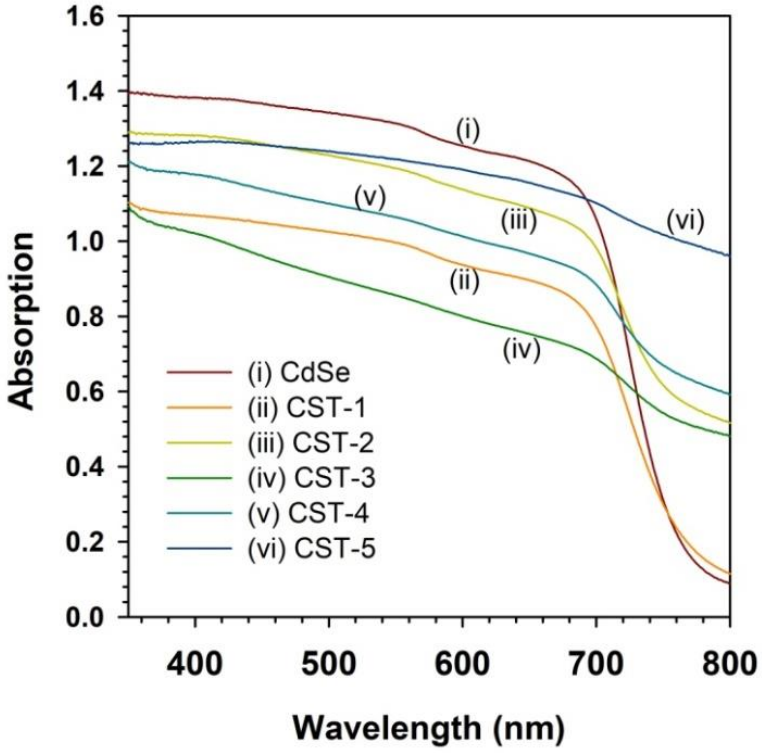

Figure 4. Diffused reflectance UV-vis spectra of CdSe and CdSe@TiO_2 for different TTIB concentrations.

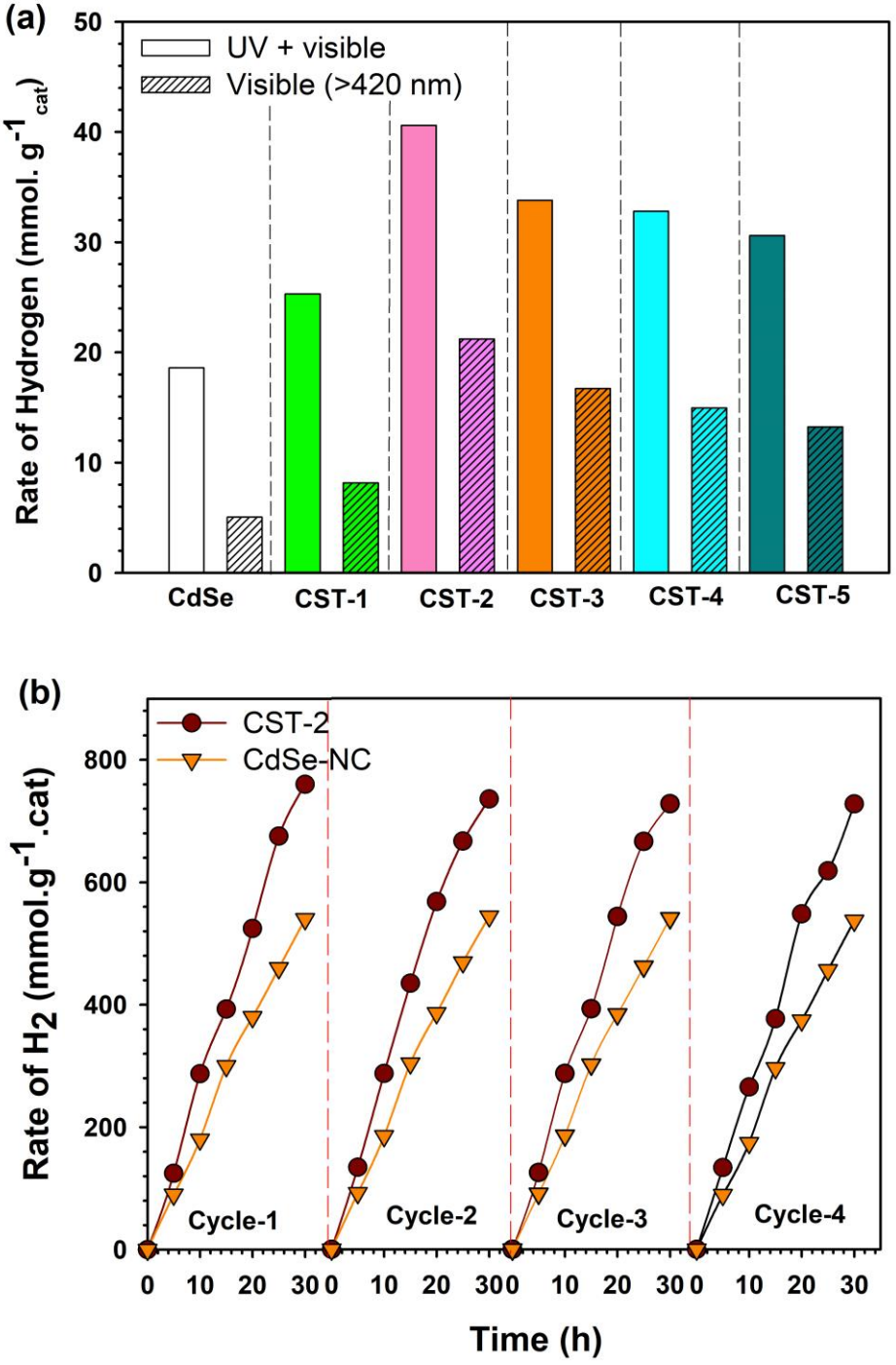

Figure 5. a) Rate of hydrogen gas evolution from photocatalysis process using CdSe and different CdSe@TiO_2 photocatalyst; b) Volume of hydrogen gas generation from different operating cycles using CST-2 photocatalyst. Note that the photocatalysis experiments were carried out at under UV + visible light irradiation, and aqueous 0.3 M Na_2S and Na_2SO_4 is used as electrolyte. In Figure 5b, dashed vertical line between each cycles indicates evacuation stage.

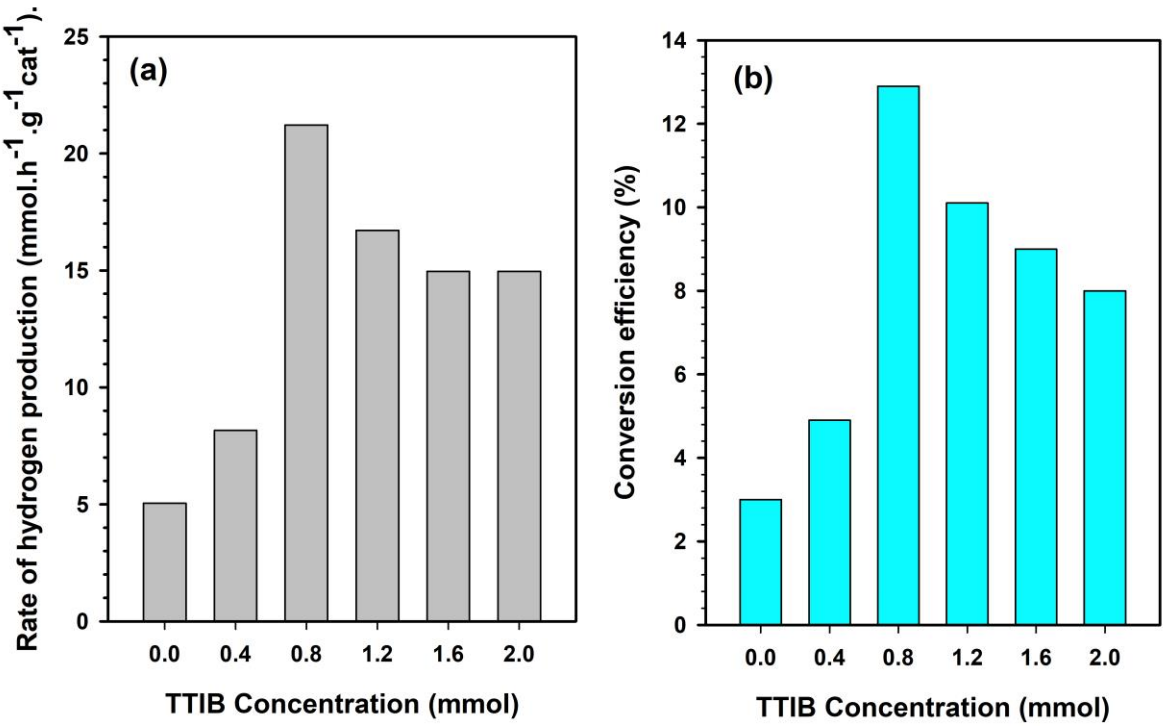

Figure 6. Influence of TTIB concentration on CdSe@TiO_2 (CST-2) photocatalytic performance; a) output hydrogen rate; b) visible light to hydrogen conversion efficiency.

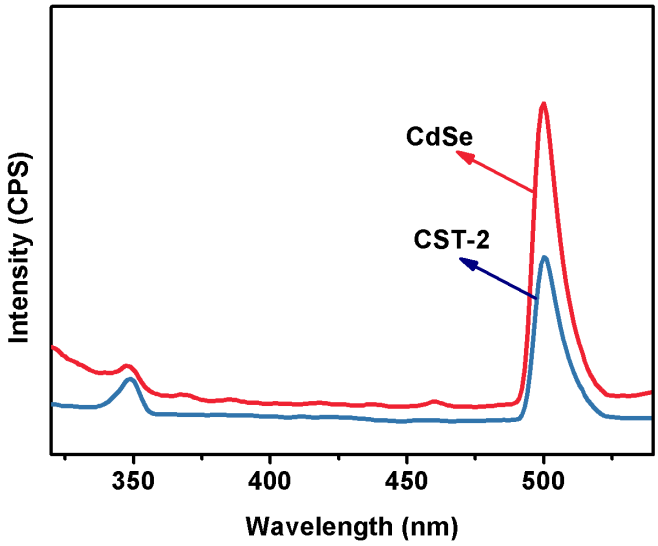

Figure 7. Photoluminescence spectra of pristine CdSe and optimized core-shell (CST-2) nanostructured photocatalyst.

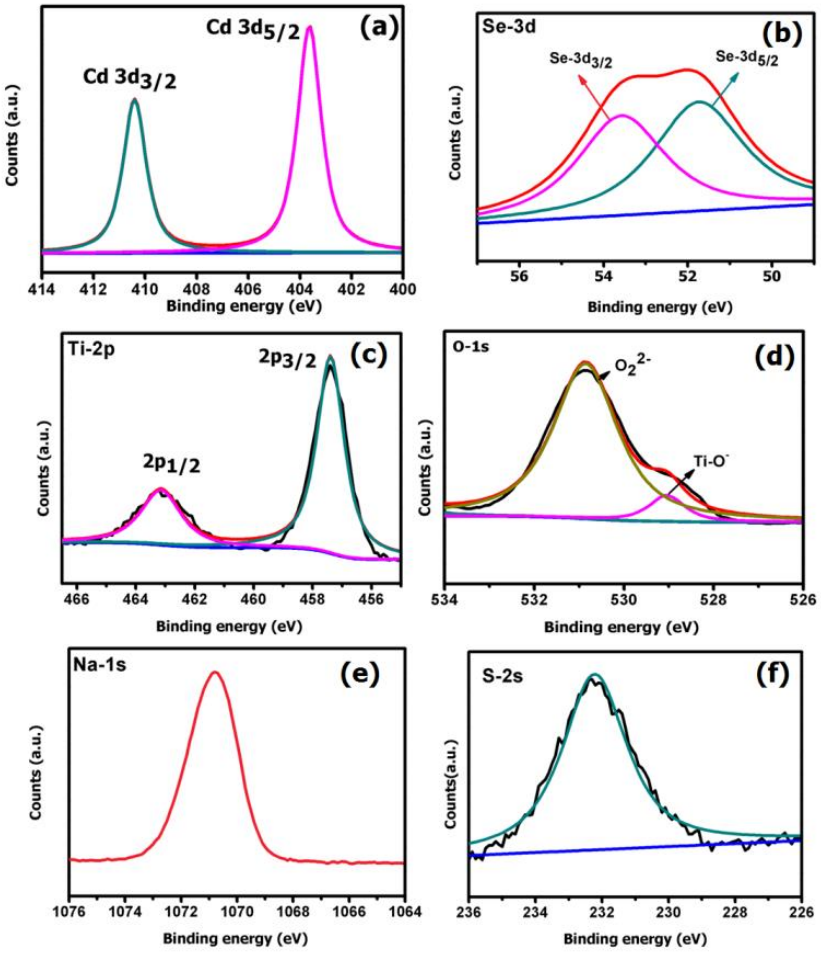

Figure 8. XPS spectrum of the used catalyst CST-2; a) Cd-3d; b) se-3d; c) Ti-2p; d) O-1s; e) Na-1s; f) S-2s peaks.

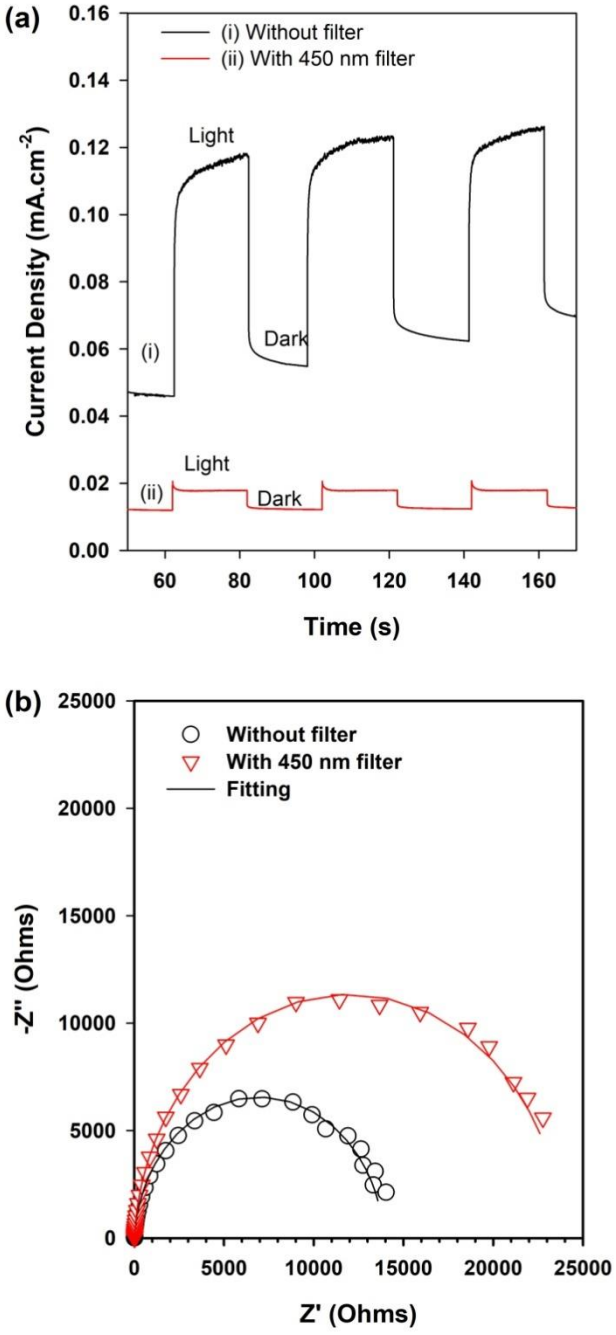

Figure 9. a) Chronoamperometry plots; b) Nyquist plots of CST-2 electrodes. Note that experiments were recorded at white light irradiation, and the experimental data is presented in symbols, and solid line indicates the fitting data].

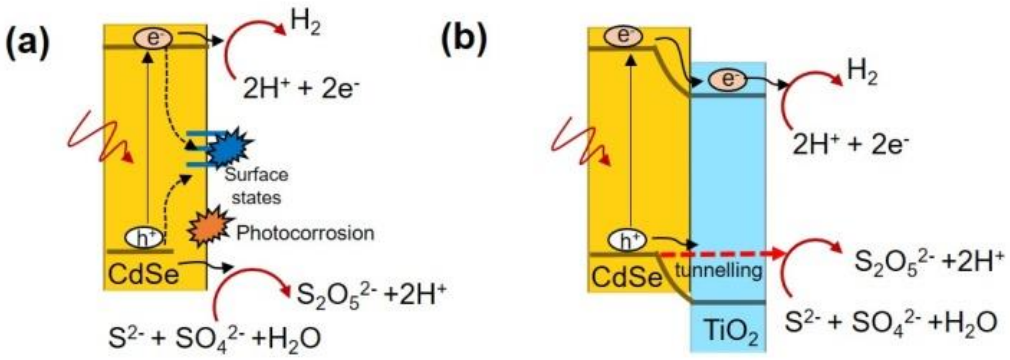

Scheme 2. Proposed charge transfer mechanism; a) CdSe; b) CdSe@TiO_2 core@shell interfaces.

Table 1. The photocatalytic hydrogen generation performance of CdSe@TiO_2 nanocapsule (present work) and compared with previous reports on CdSe based nanostructures with heterostructure, co-catalyst and passivation layer coating.

Photocatalyst	**Rate of H_2 production ($mmol.h^{-1}.g^{-1}_{cat}$)**	**Electrolyte /sacrificial agent**	**Reference**
CdSe	0.08[c]	Ethanol	[75]
CdSe	0.5 [c]	Na_2S/Na_2SO_3	[76]
CdSe QDs	0.001 [c]	Na_2SO_3	[77]
CdSe/Au	0.07 [c]	Na_2SO_3/Na_2S	[78]
CdSe QD/WS_2	14 [c]	Lactic acid	[79]
CdSe/$BaTiO_3$	2.2 [c]	Na_2S/Na_2SO_3	[80]
CdSe/CdS	0.01 [c]	Na_2S/Na_2SO_3	[29]
CdSe/CdS	0.05 [d]	Na_2S/Na_2SO_3	[81]
CdSe/CdS/Pt	12.7 [c]	Na_2S/Na_2SO_3	[82]
CdSe/CdS/ZnS	1.4 [c]	Na_2S/Na_2SO_3	[83]
CdSe/TiO_2	0.23 [b]	Na_2S/Na_2SO_3	[57]
CdSe/TiO_2	8.4[a]	Na_2S/Na_2SO_3	[84]
CdSe/CdS/TiO_2	0.45[b]	Ethylene glycol /Na_2S	[85]
CdSe/TiO_2/ $Ni(OH)_2$	10.1 [c]	Triethylamine	[86]
CdSe@TiO_2	**40.6** [d]	**Na_2S/ Na_2SO_4**	**This work**
CdSe@TiO_2	**21** [c]	**Na_2S/ Na_2SO_4**	**This work**

Light source: [a] Solar light; [b] Simulated Solar Light (AM 1.5 filter); [c] Simulate Solar Light (visible); [d] Simulate Solar Light (UV-visible).

The table of contents entry should be 50–60 words long, and the first phrase should be bold.

Photocatalyst shell thickness is the key: The nanoscale layer of TiO_2 is wrapped over CdSe nanocapsules which prevents CdSe against photocorrssion and propels photoexcitons transfer to TiO_2 surface for reactions. At optimum shell thickness, CdSe@TiO_2 shows 4 folds a high rate of H_2 production that provides its efficiency and stability for prolonged usage under recyclable conditions with TOF of 0.05018 s^{-1}.

Vempuluru Navakoteswara Rao, Sudhagar Pitchaimuthu,* Parnapalle Ravi, Marappan Sathish, Hyungkyu Han, and Shankar Muthukonda Venkatakrishnan*

Retorting Photocorrosion and Enhanced Charge Carrier Separation at CdSe Nanocapsules by Chemically Synthesized TiO_2 Shell for Photocatalytic Hydrogen Fuel Generation